

# MCVO: A Generic Visual Odometry for Arbitrarily Arranged Multi-Cameras

Huai Yu Junhao Wang Yao He Wen Yang Gui-Song Xia

**Abstract**—Making multi-camera visual SLAM systems easier to set up and more robust to the environment is always one of the focuses of vision robots. Existing monocular and binocular vision SLAM systems have narrow FoV and are fragile in textureless environments with degenerated accuracy and limited robustness. Thus multi-camera SLAM systems are gaining attention because they can provide redundancy for texture degeneration with wide FoV. However, current multi-camera SLAM systems face massive data processing pressure and elaborately designed camera configurations, leading to estimation failures for arbitrarily arranged multi-camera systems. To address these problems, we propose a generic visual odometry for arbitrarily arranged multi-cameras, which can achieve metric-scale state estimation with high flexibility in the cameras' arrangement. Specifically, we first design a learning-based feature extraction and tracking framework to shift the pressure of CPU processing of multiple video streams. Then we use the rigid constraints between cameras to estimate the metric scale poses for robust SLAM system initialization. Finally, we fuse the features of the multi-cameras in the SLAM back-end to achieve robust pose estimation and online scale optimization. Additionally, multi-camera features help improve the loop detection for pose graph optimization. Experiments on KITTI-360 and MultiCamData datasets validate the robustness of our method over arbitrarily placed cameras. Compared with other stereo and multi-camera visual SLAM systems, our method obtains higher pose estimation accuracy with better generalization ability. Our codes and online demos are available at <https://github.com/JunhaoWang615/MCVO>.

## I. INTRODUCTION

Visual Simultaneous Localization and Mapping (vSLAM) is a fundamental technique in robotics and autonomous navigation, enabling a system to estimate its motion relative to its environment using visual sensors. Traditional monocular or stereo SLAM systems often require strict camera configurations and rely heavily on integrating inertial measurement units (IMUs) for true scale pose estimation and map construction [1], [2]. However, these approaches are limited by the narrow FoV and perform poorly in environments where camera placement flexibility is paramount, such as most cars with 6 different cameras. Recently, multi-camera visual SLAM allows for greater robustness in these situations, which can cover more surrounding visual scenes to provide redundancy for poorly textured environments. It opens up

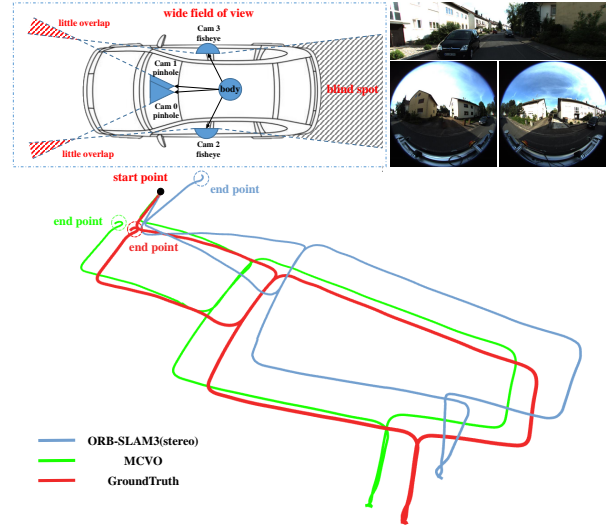


Fig. 1: Illustration of the proposed MCVO system. An example of using two fisheye and one pinhole camera on KITTI-360 dataset [5] for state estimation. The proposed MCVO obtains better performance compared with ORB-SLAM3 [2] using the front stereo camera.

new possibilities for applications such as UAV navigating through cluttered environments [3], and autonomous driving with surrounding multi-cameras [4].

However, current multi-camera visual SLAM systems still face challenges for real-world applications. On the one hand, the increase in the number of cameras, while providing information redundancy, inevitably brings several times the pressure of data processing. Most existing methods adopt conventional feature association methods, such as ORB [4], [6], which leads to a sharp increase in CPU usage and difficulty in balancing the resources for the back non-linear optimization, resulting in the requirement of high-performance CPU or failure to achieve real-time. On the other hand, accurate scale estimation is also challenging for MCVO systems. Existing methods mostly estimate the scale by multiple binocular setups or adding IMUs [7]–[9], which require elaborate configuration of the camera's FoV overlap or extrinsic calibration between camera and IMU sensors, making it difficult to balance the flexibility of the system configuration and the accuracy of the scale estimation. Therefore, the main objective of this work is to achieve robust and generalized multi-camera visual odometry by solving the feature association computation pressure and scale estimation problem for arbitrarily arranged multi-camera systems.

Huai Yu, Junhao Wang and Wen Yang are with the School of Electronic Information, Wuhan University, Wuhan, China 430072. {yuhuai, junhaoawang, yangwen}@whu.edu.cn

Yao He is with the Department of Electrical Engineering, Stanford University, Stanford, CA 94305, USA. yaohe09@stanford.edu

Gui-Song Xia are with the School of Computer Science, Wuhan University, Wuhan, China 430072. {guisong.xia}@whu.edu.cn

To address these challenges, we propose a generic multi-camera visual odometry system, *i.e.*, MCVO, which takes only multiple rigidly bundled cameras at arbitrary orientations and positions. We first analyze the state-of-the-art feature association methods from the accuracy-efficiency perspective and design a learning-based feature extraction and tracking framework to shift the computation pressure of CPU processing of multiple video streams. Then, we initialize the SLAM system to obtain true scale body poses based on the rigid constraint between the aligned poses for each camera using SfM. In the backend, we fuse multi-camera features to achieve robust pose estimation and scale optimization. The multi-camera features are further concatenated in Bag Of Words (BoW) for loop closure detection. Through rigorous testing and practical implementation on the KITTI-360 and MultiCamData datasets, we aim to demonstrate the efficacy of our system in enhancing the capabilities of autonomous agents across various domains with unprecedented levels of flexibility and generalizability. The highlights of the proposed system: (i) It enables the use of multiple cameras positioned in any orientation with only the requirement of the extrinsic parameters. (ii) By eliminating the dependency on IMU and providing the flexibility to handle cameras in arbitrary configurations, it focuses solely on visual information, no matter overlapping or non-overlapping cameras, which allows for true scale estimation and online optimization, leading to enhanced accuracy and robustness. (iii) Besides, it can accommodate a variety of camera types, including but not limited to fisheye and standard pinhole cameras, making it suitable for a broad range of applications. The main contributions are listed as follows:

- We propose a generic visual SLAM system framework for arbitrarily arranged multi-cameras, with novel designs for front-end multi-camera feature detection and matching, system initialization, back-end optimization, and loop closure.
- We comprehensively consider the existing SOTA feature association methods and design a SuperPoint-based extractor and LK tracking front-end, shifting the computational pressure of the CPU and improving the stability of feature matching, which finally provides a guarantee for the stability and efficiency of multi-eye SLAM.
- We propose a SLAM scale estimation strategy based on the trajectory consistency of multi-cameras, which is compatible with different camera models and with or without camera FoV overlap, demonstrating strong generalization and stability.

## II. RELATED WORK

### A. Efficient Feature Association Frontend

With the widespread application of multi-camera setup in SLAM systems, several times as many images need to be processed, resulting in higher CPU usage and pressure on real-time performance. Experiments on the jetson AGX Xavier [10] show that VINS-Mono consumes approximately 150-170% CPU in multi-core processing, while MSCKF exceeds 170%.

To enhance system efficiency, some approaches utilize GPUs for parallel processing, shifting the computationally intensive front-end of multi-camera systems to reduce CPU usage and latency. Common feature detectors, such as Shi-Tomasi and Harris, have been implemented in CUDA Visual Library (VILIB) [11] for fast feature extraction. He *et al.* [9] developed front-end feature tracking algorithms that run on GPUs using NVIDIA’s VPI. Additionally, learning-based methods for feature extraction and tracking [12] [13] have been proposed to enhance feature robustness while reducing the computational burden on CPU. Pandey *et al.* [14] introduced a visual odometry algorithm combining deep learning with optical flow tracking.

To further reduce CPU usage, only selecting useful features for backend optimization can improve pose estimation accuracy while lowering the computational demands. For example, RANSAC [15] is a common practice to remove obvious outliers with large reprojection errors. Scoring on the feature descriptor and uncertainty estimation using networks are also often used for selecting features for SLAM systems [16], [17]. Carlone *et al.* [18] introduced an efficient feature selection algorithm using the Max-logDet metric and minimal eigenvalue, which Zhao *et al.* [19] later improved by optimizing the feature subset selection to maximize logDet, which makes the algorithm an order of magnitude faster than state-of-the-arts. These feature selection strategies are useful for reducing the number of features for multi-camera visual odometry systems.

### B. Multiple Camera Visual Odometry

Most current VO algorithms focus on monocular and stereo cameras, such as VINS-MONO [1] and ORB-SLAM [2]. While these methods offer good performance and efficiency, they are still not robust enough for autonomous pose estimation in complex real-world environments. Multi-camera setups can significantly increase visual constraints and provide richer image information, enhancing the robustness of SLAM systems. As a result, multi-camera SLAM has gained growing attention. Early work by Sola *et al.* [20] explored multi-camera VO by fusing multiple monocular camera data using filtering methods.

More recent multi-camera SLAM systems [3], [6] extend monocular PTAM [21] and ORB-SLAM to synchronized multi-camera rigs through optimization-based approaches. Liu *et al.* [4] proposed a pose tracker and local mapper capable of supporting arbitrary numbers of stereo cameras. Tribou *et al.* [22] introduced a real-time visual odometry system utilizing multiple non-overlapping FoV cameras. This configuration provides a wider FoV, enhancing redundancy for backend optimization. However, it is challenging for non-overlapping cameras to obtain accurate scale information. To improve scale accuracy, some works adopt multi-camera setups with overlapping FoV [23] [24]. Zhao *et al.* [25] proposed an early multi-camera depth estimation method, achieving stable long-term depth estimation. Kaveti *et al.* [7] developed a multi-camera framework that extracts 3D feature points and real scale by matching overlapping areas between

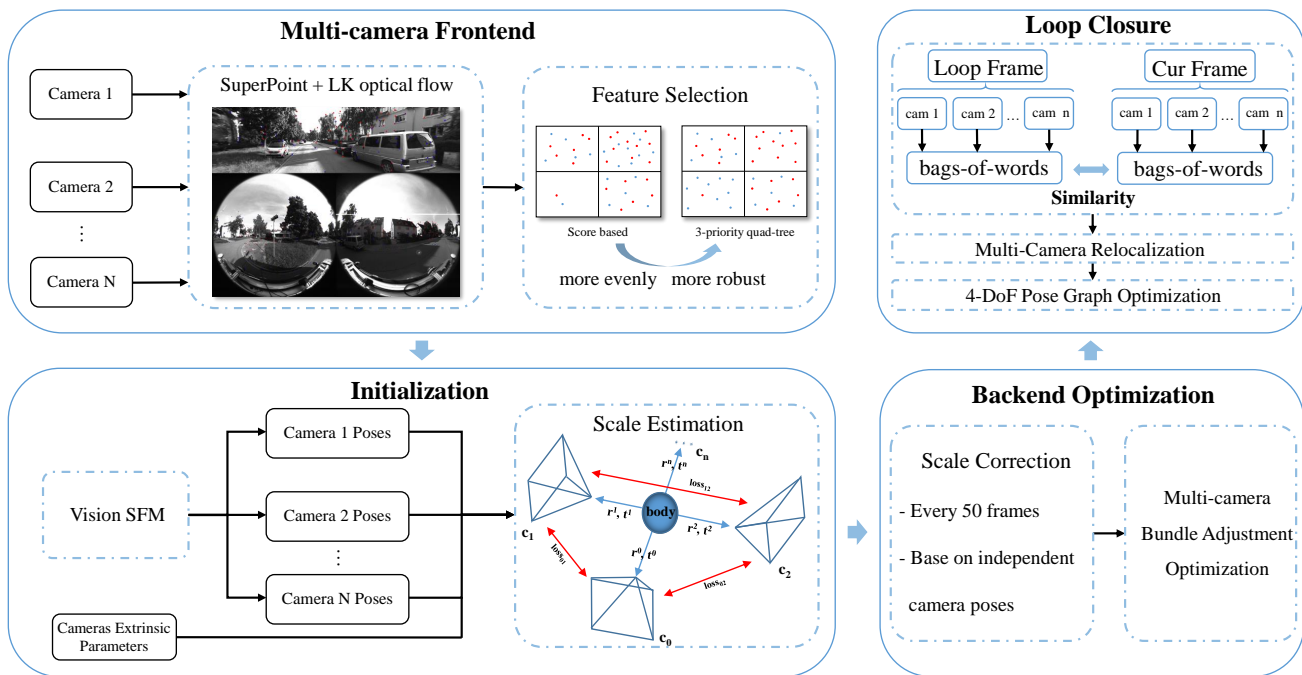


Fig. 2: The pipeline of the proposed MCVO system. Scale estimation and correction ensure scale stability.

cameras. Xu *et al.* [26] proposed a depth estimation method that does not require large FoV overlaps, enhancing depth estimation generalization across different multi-camera configurations. In addition to traditional scale estimation methods, many deep learning-based approaches have emerged [27] [28]. While these methods perform well on specific datasets, their heavy reliance on contextual information results in poor generalization in cross-dataset experiments [29].

While overlapping multi-camera setups improve the scale estimation accuracy, they do so by reducing the range of observed information, which limits the applicability of multi-camera SLAM in non-overlapping configurations. To a certain extent, this also goes against the original intention of using multi-camera systems to maximize FoV and information capture. Our proposed MCVO accurately estimates scale information based on multi-camera trajectory consistency, regardless of camera overlaps. It can be applied to arbitrarily arranged camera setups, fully leveraging the wide FoV advantages of multi-camera systems.

### III. METHODOLOGY

#### A. Overview

Our proposed generic multi-camera visual odometry framework is illustrated in Fig. 2. The main inputs to the framework are the synchronized multi-camera video sequences. The multiple cameras are rigidly bundled and calibrated in advance with known intrinsic and extrinsic parameters. The output is the metric scale 6-DoF robot poses in the real-world environment. The pipeline comprises four components: frontend feature extraction, pose and metric scale initialization, backend optimization, and loop closure. To accelerate the frontend of multi-camera feature association, we employ feature extraction with GPU

acceleration and 3-priority feature selection (Section III-B). Then we initialize the multi-camera system of metric scale body poses using the multi-camera poses and extrinsic parameters (Section III-C). To ensure the realism of the motion scale, we perform an adaptive correlation of the scale deviations during the backend optimization (Section III-D). Given the larger FoV of the multi-camera system, we design a more robust multi-camera omnidirectional loop detection algorithm (Section III-E). We further optimize the body poses in the loop with the pose graph constraint.

#### B. Efficient Multi-Camera Frontend

The frontend of our proposed MCVO primarily processes multi-camera images, extracts and matches useful features, and then provides reliable landmarks for the backend optimization.

Improving feature detection quality and association efficiency are essential for the visual odometry frontend. As the number of cameras increases, the volume of extracted and tracked features grows significantly, leading to a considerable computational burden for real-time performance. Regarding these issues, we utilize SuperPoint [30] for feature extraction and LK optical flow for feature tracking. This process is accelerated via GPU, substantially reducing CPU usage brought by multiple cameras and enhancing performance in handling image streams.

We further conduct a feature selection process, to reduce the CPU load during optimization and improve estimation performance. The traditional quad-tree algorithm [31] tends to place new features close to existing features in texture-rich regions, which might reduce the optimization accuracy due to insufficient constraints. Our feature selection algorithm avoids excessive feature concentration to ensure an even distribution of features through three key priorities.

- 1) Quantity priority: Prioritizes nodes with more features to enhance processing efficiency.
- 2) Tracked feature priority: Prioritizes reducing the density of points in texture-rich areas by avoiding adding useless features near tracked points.
- 3) High score feature priority: Prioritizes features with higher scores.

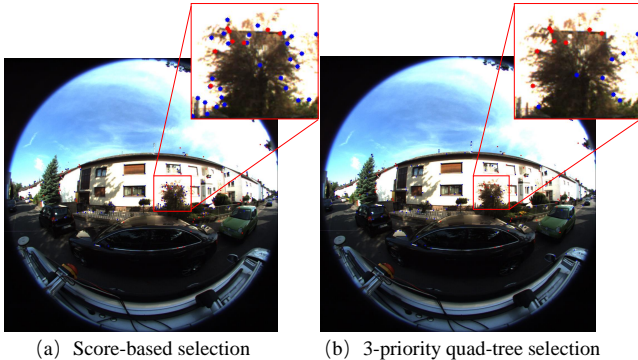


Fig. 3: Distribution of feature points. The proposed approach achieves more uniform feature distribution and better robustness than the score-based method. *Red points*: tracked features. *Blue points*: newly added features.

### C. Multi-Camera Initialization

The initialization of our MCVO system aims to estimate initial poses and determine the metric scale of motions. This process includes the pose initialization for each camera and metric scale estimation for body poses.

We first calculate the parallax for each camera in a 10-frame window. When all the camera frames at time  $t$  have sufficient parallax (greater than 30 pixels), we set the world coordinate origin at time  $t$  for all cameras. The camera with the most tracking features at time  $t$  is selected as the principal camera. Simultaneously, we estimate the poses for each camera independently using Structure from Motion (SfM) on the landmarks provided by the frontend for the 10 frames in the initialization window. It should be noted that the SfM is conducted on 10 frames of each monocular camera, therefore, the scale of each camera is not on the same metric level.

Subsequently, given the poses for all cameras, we first calculate the body frame (principal camera frame) poses using the camera extrinsic parameter

$$\mathbf{p}_t^{b_c} = \mathbf{R}_t^c \mathbf{p}_t^c + s^c \mathbf{p}_t^c, \quad (1)$$

where  $\mathbf{R}_t^c$ ,  $\mathbf{p}_t^c$  are the estimated rotation and translation for camera  $c$  at timestamp  $t$ ,  $s^c$  is the scale parameter for camera  $c$  to be estimated,  $\mathbf{p}_t^c$  is the translational extrinsic parameter of camera  $c$  and  $\mathbf{P}_t^{b_c}$  is the body frame translation estimated from camera  $c$  at timestamp  $t$ .

However, because each camera's pose is computed independently, their scales are not aligned, resulting in significant discrepancies in body poses. Theoretically, the estimated body pose should be consistent across different cameras. Therefore, we take the differences between body poses

calculated by different cameras as the residuals and define the optimization problem as follows:

$$\min_{s_1, s_2, \dots, s_{n_c}} \sum_t \sum_{i=1}^{n_c} \sum_{j=i+1}^{n_c} \|\mathbf{p}_t^{b_i} - \mathbf{p}_t^{b_j}\|^2, \quad (2)$$

where  $n_c$  is the number of cameras,  $s_k (k \in [1, n_c])$  is the scale parameter for camera  $k$ ,  $\mathbf{P}_t^{b_c}$  is the body frame translation estimated from camera  $k$  at timestamp  $t$ . To solve the least squares problem for Eq. (2), we use the Levenberg-Marquardt algorithm from the Ceres Solver library [32].

We readjust camera poses according to the estimated metric scale, then re-triangulate all features using the updated poses to obtain their metric depths. After the initial estimation of poses and scales, we proceed with a sliding window-based backend optimization for state estimation.

### D. Scale Correction and Backend Optimization

After initializing the pose estimation system with metric scale. We use a vision-only bundle adjustment with the extracted features from all cameras to minimize the sum of prior and the Mahalanobis norm of all visual measurement residuals to obtain a maximum posterior state estimation,

$$\min_{\mathcal{X}} \left\{ \|\mathbf{r}_0\|_{\Sigma_0}^2 + \sum_{i \in \mathcal{C}} \sum_{j \in \mathcal{F}_i} \rho(\|\mathbf{r}_{v(i,j)}\|_{\Sigma_{v(i,j)}}^2) \right\} \quad (3)$$

$$\mathcal{X} = [\mathbf{x}_1^b, \mathbf{x}_2^b, \dots, \mathbf{x}_t^b, \lambda_1, \lambda_2, \dots, \lambda_{n_c}]$$

where the state vector  $\mathcal{X}$  includes the body poses  $\mathbf{x}_t^b$  in the sliding window and all the feature depths  $\lambda_c$  observed by the  $c$ -th camera,  $\rho(\cdot)$  is the robust huber loss,  $\mathcal{C}$  is the set of cameras,  $\mathcal{F}_i$  is the set of reliable features in  $i$ -th camera,  $\mathbf{r}_0$  is the marginalization factor,  $\mathbf{r}_{v(i,j)}$  is the  $j$ -th landmark reprojection residual in the  $i$ -th camera. The definition of all the residuals can be found in [1]. The Dogleg algorithm in the Ceres Solver [32] is employed to solve this least squares problem.

**Scale Correction.** The optimization in Eq. (3) continuously provides accurate body poses and feature depths. However, scale error gradually accumulates as the map expands. To address this, we conduct scale correction alongside the backend optimization at regular intervals. During scale correction, a vision-only bundle adjustment is first performed for each camera to determine its poses independently of the body. We then apply the scale estimation algorithm described in Section III-C to obtain the scale factors  $s$ . Instead of directly adjusting the pose scales, we modify the feature depths in each camera, allowing for a smoother scale correction of poses through subsequent state estimation.

### E. Multi-Camera Loop Closure

Although the multi-camera VO and scale correction provide high-accuracy state estimation, the accumulated drifts still exist alongside the running of pure visual odometry. To mitigate the drifts over time, we design a multi-camera loop closure module across different cameras and establish loop connections in the pose graph for further state optimization.

**Loop Detection.** In our MCVO pipeline, the loop detection simply leverages DBoW2 [33] algorithm for place recognition. The key point is how to use multi-camera features to improve the loop detection accuracy and robustness. Firstly, the features from all cameras are stored in the corresponding bag-of-words model. Then potential loop frames are identified by comparing matching scores between DBoW2 models from different frames. The wide field of view offered by multi-camera setups improve the detection rate of potential loops.

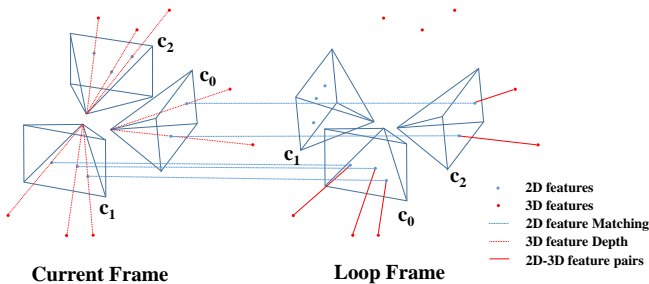


Fig. 4: Illustration of the multi-camera re-localization

Upon detecting a loop, we proceed with re-localization as illustrated in Fig. 4. The current frame features are converted into 3D features  $z$  with their depth information. By matching feature descriptors from the looped frames, we establish 2D-3D feature correspondences  $\{(x_i, z_i)\}$ . When a camera has sufficient 2D-3D feature pairs, we proceed with the following optimization to refine camera poses

$$\min_{\mathcal{R}, \mathcal{P}} \sum_c \sum_i \|\mathbf{x}_i - \pi(\mathbf{K}_c, z_i, \mathbf{R}, \mathbf{p})\|^2, \quad (4)$$

where  $\mathbf{K}_c$  is the intrinsic and the extrinsic (to body frame) parameters of camera  $c$ ,  $\pi$  is the projection of the  $z_i$  on the image plane. The least squares problem is also solved by the Levenberg-Marquardt algorithm.

This process ensures accurate re-localization even with significant viewpoint differences. If multiple cameras meet the criteria, we use extrinsic constraints to verify the re-localization’s success further. Once verified, the accurate body pose of the loop frame is determined based on the camera poses and extrinsic parameters. Compared to a monocular system, our multi-camera setup enhances loop detection from different viewpoints, significantly increasing the detection rate of loops.

**Pose Graph Optimization** We follow the commonly used 4-DoF pose graph optimization [1] to update the trajectory in the loops. The pose graph  $\mathcal{G} = \{\mathbf{V}, \mathbf{E}\}$  keep track of all keyframes with their spatial constraints, where vertices  $\mathbf{V}$  represent keyframes and edges  $\mathbf{E}$  store the transformation constraints between keyframe poses. Keyframes marginalized during the sliding window are added to the pose graph, with their relative transformations to other keyframes in the local sliding window incorporated as edges. When a loop is detected, a loop edge between the current frame and the loop frame is added to  $\mathbf{E}$ , followed by the 4-DoF pose graph

optimization. The optimization process effectively reduces accumulated errors and enhances the system’s robustness.

## IV. EXPERIMENTS

In this section, we conduct experiments on two public datasets to evaluate our proposed method.

### A. Experimental Setup

1) *Datasets:* For the evaluation of our method, the dataset must contain multi-camera setup with pre-calibrated intrinsic and extrinsic parameters. We select two public available dataset, *i.e.*, KITTI360 [5] and MultiCamData [7], which have different camera types, scenario types, and various camera layouts. The KITTI360 dataset was collected in outdoor road environments with two 180° fisheye cameras and two 90° pinhole cameras, as shown in Fig. 1. The four cameras are synchronized and pre-calibrated. Compared to other datasets such as EuRoC [34], KITTI360 features larger scale, longer distances, and challenging scenarios, such as roads under bridges (lighting changes), wilderness (texture degradation), and dynamic scenes. We tested on most of the sequences and compared with the ground truth trajectories. MultiCamData was collected in indoor environments using 6 cameras. We mainly use the non-overlapping cameras (cam0, cam5, and cam6) for generalizability. The dataset also includes challenging scenarios, such as narrow corridors, large white walls (texture degradation), sudden turns, and dynamic scenes.

2) *Evaluation Setup:* We select VINS-Fusion [1], ORB-SLAM3 [2], and MultiCamSLAM [7] as baselines for comparison. To obtain metric scale state estimation for VINS-Fusion and ORB-SLAM3, these two methods are setup with front stereo cameras of each dataset. While for MultiCamSLAM, we employ a non-overlapping camera setup consistent with the method [7]. MCVO is configured with two fisheye cameras and one front pinhole camera on KITTI360 dataset. The evaluation metrics on KITTI360 include Absolute Trajectory Error (ATE), Relative Pose Error (RPE) and scale error [35]. Since MultiCamData lacks ground truth trajectory, we estimate the errors between the initial and final poses using a visual target as in [7], given that the start and end of the trajectories are at the same location. All the experiments are conducted on a desktop with a 2.5GHz Intel Core i7-11700 CPU and an NVIDIA RTX3060 GPU.

### B. Experimental Results

The quantitative results for ATE are presented in Table I and Fig. 5. Compared with the stereo ORB-SLAM3 and VINS-Fusion, MCVO achieves significantly lower rotation error and competitive translation error on most of the sequences of KITTI360, primarily due to the wide FoV provided by the multi-camera setup and the high accuracy and robustness of the frontend. The small scale errors further demonstrate the effectiveness of our scale estimation strategy. The MultiCamSLAM method cannot finish most of the sequences on KITTI360. This issue arises because the KITTI360 dataset was captured at high speeds, leading to

TABLE I: Comparison of ATE on various datasets. The metrics translation, rotation, and scale are in meters, degrees, and percentages, respectively. Note that MultiCamSLAM fails after running a certain distance (as shown in parentheses) on the KITTI360.

Method	KITTI360_00 (1520m)			KITTI360_03 (1379m)			KITTI360_05 (1173m)			KITTI360_10 (3343m)			MCdata_Lab1 (152m)		MCdata_Ground1 (90m)	
	Trans.	Rot.	Scal.	Trans.	Rot.	Scal.	Trans.	Rot.	Scal.	Trans.	Rot.	Scal.	Trans.	Trans.	Trans.	Trans.
VINS-Fusion	76.198	114.923	1.003	38.213	125.079	0.585	14.749	123.580	0.181	135.536	130.248	2.924	16.579	10.921%	14.80	16.469%
ORB_SLAM3	<u>22.673</u>	117.981	<u>0.390</u>	<b>12.269</b>	115.832	<b>0.306</b>	8.134	114.361	<u>0.164</u>	<b>44.317</b>	114.268	<b>1.484</b>	<b>2.90</b>	<b>1.91%</b>	<b>0.85</b>	<b>0.80%</b>
MultiCamSLAM	15.68(245.2)	115.516	0.341	8.91(222.5)	114.082	0.184	11.28(91.9)	155.944	0.150	56.46(553.5)	136.175	1.561	14.83	9.75%	1.69	1.88%
MCVO(ORB)	44.054	<u>8.634</u>	0.518	64.861	<u>4.803</u>	1.367	49.143	<u>5.353</u>	0.591	102.050	<u>6.139</u>	2.833	11.50	7.561%	14.58	16.321%
MCVO(ours)	<b>13.933</b>	<b>6.847</b>	<b>0.300</b>	<u>20.234</u>	<b>2.585</b>	<u>0.394</u>	<b>6.895</b>	<b>3.341</b>	<b>0.079</b>	<u>76.282</u>	<b>7.348</b>	<u>2.638</u>	7.894	<u>5.200%</u>	<u>1.54</u>	<u>1.711%</u>

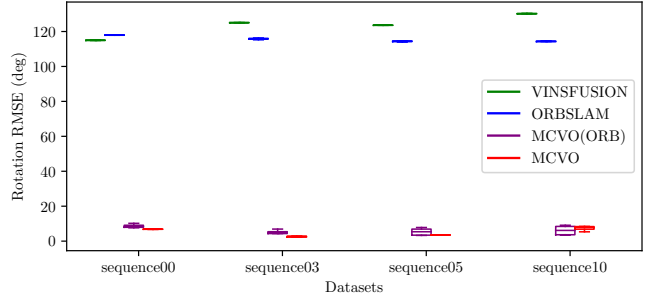
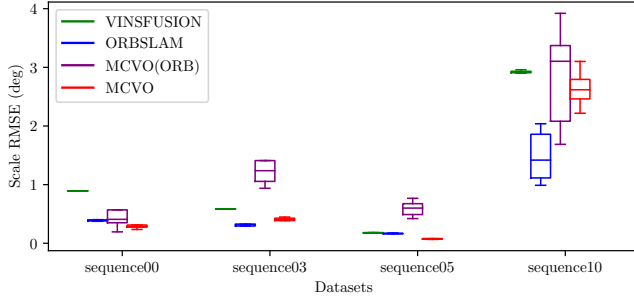


Fig. 5: Comparison of ATE for different methods on the KITTI360

large inter-frame displacements. MultiCamSLAM struggles with significant inter-frame displacements, hindering triangulation and initialization. The comparison with MCVO on ORB features further shows the robustness of our frontend design. Besides, MCVO shows strong performance and robustness on MultiCamData. It outperforms VINS-Fusion in accuracy, with a marginal shortfall compared to ORBSLAM3. This slight reduction in accuracy is primarily attributed to the presence of numerous white walls in indoor corridors, which introduce noise that impacts multi-camera VO. Compared to MultiCamSLAM, which also employs a non-overlapping camera setup, MCVO achieves superior accuracy and better generalization across different sequences.

Fig. 6 presents the RPE results of different methods on the 00 sequence of KITTI360 dataset. MCVO significantly outperforms other methods with smallest pose drift. This improvement is largely due to the wide coverage of scenes in the multi-camera setup with a robust and efficient frontend. The expanded FoV offers stronger constraints for state estimation, resulting in higher pose estimation accuracy. Additionally, the robust frontend ensures accurate feature tracking even in low-quality scenes. These results validate the effectiveness of MCVO on state estimation.

To further qualitative analyze the performance, we plot the trajectories of different methods on sequences 00 and 05 of KITTI360 dataset in Fig. 7. ORB-SLAM3 and VINS-Fusion exhibit large rotation errors on the 00 sequence. In contrast, MCVO shows improved stability and accuracy under such conditions. Additionally, the overall trajectory of our approach is smoother with more stable position estimation.

### C. Ablation Study

In this section, we conduct ablation experiments for different numbers of cameras, feature extractors, feature matching, and whether to use loop closure. The effectiveness

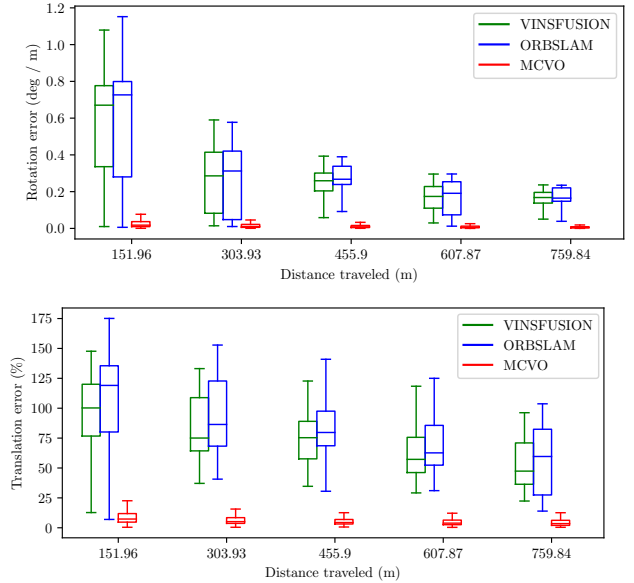


Fig. 6: Comparison of RPE for different methods on the KITTI360\_00 sequence.

of each part of our proposed method is verified through comprehensive analyses.

TABLE II: MCVO performance under different number of cameras on the KITTI360 00 sequence.

Method	Transl.[m]		Rot.[°]		Usage <sub>CPU</sub> [%]
	Mean	Std	Mean	Std	Mean
2 cams	45.523	43.042	8.180	7.263	<b>203.2</b>
3 cams	<b>13.933</b>	13.640	<b>6.847</b>	6.806	316.7
4 cams	20.673	22.262	7.671	7.812	443.6

1) *Camera number*: Table II shows the state estimation accuracy of MCVO under different number of cameras. MCVO on two cameras obtains relatively lower accuracy due to the limited FoV, which provides insufficient information.

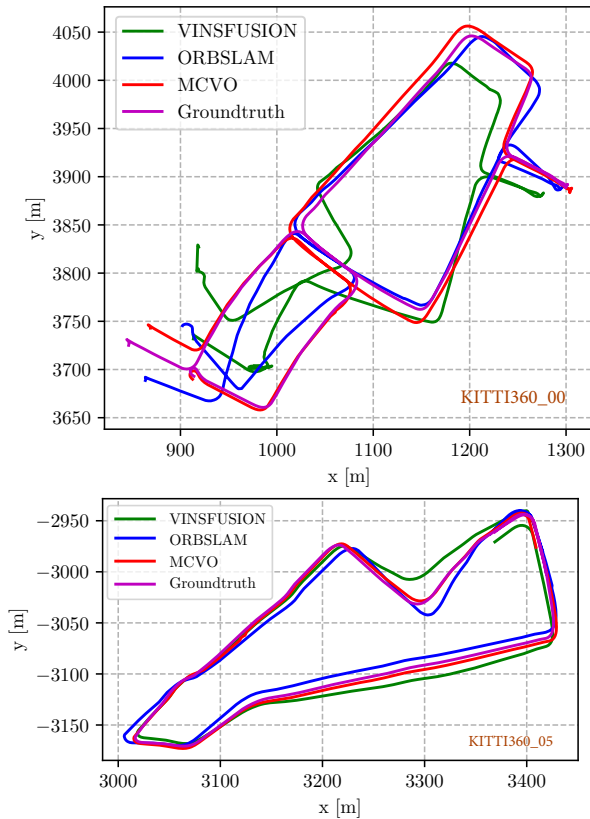


Fig. 7: Trajectories of different sequences on KITTI360.

When the number of cameras increases to 3, the estimation accuracy reaches its peak. However, with 4 cameras, there is a slight decrease in accuracy. This is primarily because two fisheye and one perspective cameras have already covered enough surrounding information, the added new camera will bring more observation noises and computational burden for the system. Consequently, the gain from the new camera cannot contribute to improving accuracy.

TABLE III: MCVO performance under different feature extractors on the KITTI360 00 sequence.

Method	Transl.[m]		Rot.[°]		Usage <sub>CPU</sub> [%]	FPS
	Mean	Std	Mean	Std	Mean	
Shi-Tomasi	39.390	40.612	9.256	8.290	398.3	18.75
ORB	44.054	39.900	8.634	8.327	942.4	12.74
SuperPoint	<b>13.933</b>	13.640	<b>6.847</b>	6.806	<b>316.7</b>	<b>19.50</b>

2) *Feature extractor*: We use pose accuracy and CPU usage metrics to compare different feature extraction methods. Table III shows that SuperPoint achieves the highest accuracy compared with commonly used Shi-Tomasi and ORB. This is mainly because SuperPoint can extract multi-level features and is more robust to environmental changes. Additionally, the CPU usage of MCVO(SuperPoint) is significantly lower. This reduction in CPU usage is because of our GPU-accelerated frontend. Consequently, The shift of CPU usage also ensures the computation resource for back-end optimization of accurate pose estimation and efficiency.

3) *Feature matching*: Table IV shows the performance of MCVO on different feature-matching methods. Flow-based

methods exhibit lower CPU usage and more inliers compared to matching-based methods (KNN, SuperGlue). Additionally, we count the mean tracking times of each feature. LK shows the longest tracking times compared to others, which provides stable landmarks for the backend pose estimation. The small number of track times of other methods leads to the pose initialization failures.

TABLE IV: MCVO performance under different feature matching methods (Superglue-SG).

Method	Inlier		Usage <sub>CPU</sub>	Aver. track	Initialization
	Num	ratio	Mean	times	succ.
ORB+KNN	51.33	34.22%	892.03%	2.71	×
ORB+LK	93.04	62.03%	750.78%	15.95	✓
SuperPoint+SG	65.23	43.39%	789.53%	4.32	×
SuperPoint+LK	<b>99.61</b>	<b>66.41%</b>	<b>710.12%</b>	<b>16.40</b>	✓

4) *Loop closure*: We also conduct experiments on the KITTI360 05 sequence to validate the effectiveness of the loop closure. The qualitative results are shown in Fig. 8. We can observe that the multi-camera loop closure effectively performs loop detection and closure, providing stable global constraints for back-end optimization. MCVO successfully corrects the cumulative error in the map, achieving more precise trajectory estimation.

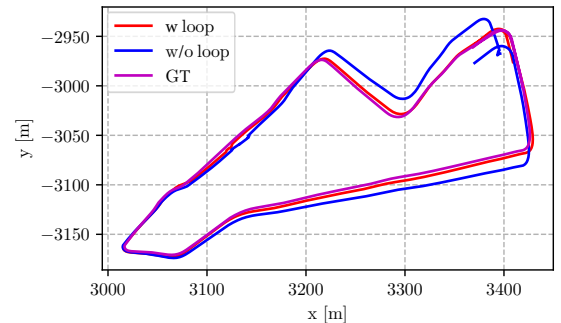


Fig. 8: Loop closure effectiveness validation on the KITTI360 05 sequence.

#### D. Discussion

The comparison with other stereo VO and multi-camera VO demonstrates the effectiveness of the proposed MCVO on state estimation. The analyses of each component validate the reasonableness of our design on multi-camera data processing. However, there are still limitations:

- Multi-camera configurations can improve VO robustness, but inevitably introduce new computational requirements. Our approach uses learning-based feature extraction to shift CPU consumption but introduces the need for GPU resources. The best approach may be to develop a specialized camera with feature association embedded in the sensor hardware.
- MCVO requires the extrinsic parameters of arbitrarily arranged multi-cameras. When there is no overlap between FoV, the extrinsic calibration will be a challenging problem.

## V. CONCLUSIONS AND FUTURE WORK

In this paper, we propose a generic multi-camera visual odometry system, which has high flexibility on the camera setup with different camera types, with or without FoV overlap. The arbitrary arrangement of multi-cameras, not only improves the flexibility of the SLAM system but also achieves robust camera-only true-scale pose estimation. The designed learning-based feature association front-end utilizes GPU to effectively release the computational pressure of CPUs on multi-camera data processing and improves the stability of feature matching. The system functionalities of multi-camera features for scale initialization, back-end optimization, and loop closure are fully validated during the experiments. Comparisons with the state-of-the-art further demonstrate the effectiveness and robustness of MCVO on state estimation. Future work will focus on the deployment of MCVO on more platforms.

## REFERENCES

- [1] T. Qin, P. Li, and S. Shen, "VINS-Mono: A robust and versatile monocular visual-inertial state estimator," *IEEE Transactions on Robotics*, vol. 34, no. 4, pp. 1004–1020, 2018.
- [2] C. Campos, R. Elvira, J. J. G. Rodríguez, J. M. Montiel, and J. D. Tardós, "ORB-SLAM3: An accurate open-source library for visual, visual-inertial, and multimap slam," *IEEE Transactions on Robotics*, vol. 37, no. 6, pp. 1874–1890, 2021.
- [3] A. Harmat, M. Trentini, and I. Sharf, "Multi-camera tracking and mapping for unmanned aerial vehicles in unstructured environments," *Journal of Intelligent and Robotic Systems*, vol. 78, p. 291–317, 2015.
- [4] P. Liu, M. Geppert, L. Heng, T. Sattler, A. Geiger, and M. Pollefeys, "Towards robust visual odometry with a multi-camera system," in *IEEE/RSJ International Conference on Intelligent Robots and Systems (IROS)*, 2018, pp. 1154–1161.
- [5] Y. Liao, J. Xie, and A. Geiger, "KITTI-360: A novel dataset and benchmarks for urban scene understanding in 2D and 3D," *IEEE Transactions on Pattern Analysis and Machine Intelligence*, vol. 45, no. 3, pp. 3292–3310, 2022.
- [6] S. Urban and S. Hinz, "Multicol-slam - a modular real-time multi-camera slam system," in *arXiv preprint arXiv:1610.07336*, 2016.
- [7] P. Kaveti, S. N. Vaidyanathan, A. T. Chelvan, and H. Singh, "Design and evaluation of a generic visual slam framework for multi-camera systems," *IEEE Robotics and Automation Letters*, 2023.
- [8] J. Jaekel, J. G. Mangelson, S. Scherer, and M. Kaess, "A robust multi-stereo visual-inertial odometry pipeline," in *IEEE/RSJ International Conference on Intelligent Robots and Systems (IROS)*, 2020, pp. 4623–4630.
- [9] Y. He, H. Yu, W. Yang, and S. Scherer, "Towards robust visual-inertial odometry with multiple non-overlapping monocular cameras," in *IEEE/RSJ International Conference on Intelligent Robots and Systems (IROS)*, 2022, pp. 9452–9458.
- [10] J. Jeon, S. Jung, E. Lee, D. Choi, and H. Myung, "Run your visual-inertial odometry on nvidia jetson: Benchmark tests on a micro aerial vehicle," *IEEE robotics and automation letters*, vol. 6, no. 3, pp. 5332–5339, 2021.
- [11] B. Nagy, P. Foehn, and D. Scaramuzza, "Faster than fast: Gpu-accelerated frontend for high-speed vio," in *IEEE/RSJ International Conference on Intelligent Robots and Systems (IROS)*, 2020, pp. 4361–4368.
- [12] S. Wang, R. Clark, H. Wen, and N. Trigoni, "DeepVO: Towards end-to-end visual odometry with deep recurrent convolutional neural networks," in *IEEE International Conference on Robotics and Automation (ICRA)*, 2017, pp. 2043–2050.
- [13] P. Muller and A. Savakis, "Flowdometry: An optical flow and deep learning based approach to visual odometry," in *IEEE Winter Conference on Applications of Computer Vision (WACV)*, 2017, pp. 624–631.
- [14] T. Pandey, D. Pena, J. Byrne, and D. Moloney, "Leveraging deep learning for visual odometry using optical flow," *Sensors*, vol. 21, no. 4, p. 1313, 2021.
- [15] M. A. Fischler and R. C. Bolles, "Random sample consensus: a paradigm for model fitting with applications to image analysis and automated cartography," *Communications of the ACM*, vol. 24, no. 6, pp. 381–395, 1981.
- [16] P. Laddha, O. J. Omer, G. S. Kalsi, D. K. Mandal, and S. Subramoney, "Descriptor scoring for feature selection in real-time visual slam," in *IEEE International Conference on Image Processing (ICIP)*, 2020, pp. 2601–2605.
- [17] P. Ganti and S. L. Waslander, "Network uncertainty informed semantic feature selection for visual slam," in *16th Conference on Computer and Robot Vision (CRV)*, 2019, pp. 121–128.
- [18] L. Carlone and S. Karaman, "Attention and anticipation in fast visual-inertial navigation," *IEEE Transactions on Robotics*, vol. 35, no. 1, pp. 1–20, 2018.
- [19] Y. Zhao and P. A. Vela, "Good feature matching: Toward accurate, robust vo/vslam with low latency," *IEEE Transactions on Robotics*, vol. 36, no. 3, pp. 657–675, 2020.
- [20] J. Sola, A. Monin, M. Devy, and T. Vidal-Calleja, "Fusing monocular information in multicamera SLAM," *IEEE Transactions on Robotics*, vol. 24, no. 5, pp. 958–968, 2008.
- [21] G. Klein and D. Murray, "Parallel tracking and mapping for small ar workspaces," in *IEEE and ACM International Symposium on Mixed and Augmented Reality*, 2007, pp. 225–234.
- [22] M. J. Tribou, A. Harmat, D. W. Wang, I. Sharf, and S. L. Waslander, "Multi-camera parallel tracking and mapping with non-overlapping fields of view," *International Journal of Robotics Research*, vol. 34, p. 1480–1500, 2015.
- [23] L. Heng, G. H. Lee, and M. Pollefeys, "Self-calibration and visual slam with a multi-camera system on a micro aerial vehicle," *Autonomous robots*, vol. 39, no. 3, pp. 259–277, 2015.
- [24] L. Heng, B. Choi, Z. Cui, M. Geppert, S. Hu, B. Kuan, P. Liu, R. Nguyen, Y. C. Yeo, A. Geiger, et al., "Project autovision: Localization and 3d scene perception for an autonomous vehicle with a multi-camera system," in *IEEE International Conference on Robotics and Automation (ICRA)*, 2019, pp. 4695–4702.
- [25] C. Zhao, B. Fan, J. Hu, L. Tian, Z. Zhang, S. Li, and Q. Pan, "Pose estimation for multi-camera systems," in *IEEE International Conference on Unmanned Systems (ICUS)*, 2017, pp. 533–538.
- [26] J. Xu, X. Liu, Y. Bai, J. Jiang, K. Wang, X. Chen, and X. Ji, "Multi-camera collaborative depth prediction via consistent structure estimation," in *30th ACM International Conference on Multimedia*, 2022, pp. 2730–2738.
- [27] M. Liu, S. Wang, Y. Guo, Y. He, and H. Xue, "Pano-sfmlearner: Self-supervised multi-task learning of depth and semantics in panoramic videos," *IEEE Signal Processing Letters*, vol. 28, pp. 832–836, 2021.
- [28] K. Zhou, K. Yang, and K. Wang, "Panoramic depth estimation via supervised and unsupervised learning in indoor scenes," *Applied optics*, vol. 60, no. 26, pp. 8188–8197, 2021.
- [29] Z. Li and N. Snavely, "Megadepth: Learning single-view depth prediction from internet photos," in *IEEE Conference on Computer Vision and Pattern Recognition*, 2018, pp. 2041–2050.
- [30] D. DeTone, T. Malisiewicz, and A. Rabinovich, "Superpoint: Self-supervised interest point detection and description," in *IEEE Conference on Computer Vision and Pattern Recognition Workshops*, 2018, pp. 224–236.
- [31] R. A. Finkel and J. L. Bentley, "Quad trees a data structure for retrieval on composite keys," *Acta informatica*, vol. 4, pp. 1–9, 1974.
- [32] S. Agarwal, K. Mierle, et al., "Ceres solver—a large scale non-linear optimization library," 2019.
- [33] D. Gálvez-López and J. D. Tardós, "Bags of binary words for fast place recognition in image sequences," *IEEE Transactions on Robotics*, vol. 28, no. 5, pp. 1188–1197, 2012.
- [34] M. Burri, J. Nikolic, P. Gohl, T. Schneider, J. Rehder, S. Omari, M. W. Achtelik, and R. Siegwart, "The EuRoC micro aerial vehicle datasets," *The International Journal of Robotics Research*, vol. 35, no. 10, pp. 1157–1163, 2016.
- [35] Z. Zhang and D. Scaramuzza, "A tutorial on quantitative trajectory evaluation for visual(-inertial) odometry," in *IEEE/RSJ International Conference on Intelligent Robots and Systems (IROS)*, 2018, pp. 7244–7251.